

# Threshold and Efficiency for Perforation of 1 nm Thick Carbon Nanomembranes with Slow Highly Charged Ions

Richard A. Wilhelm<sup>1</sup>, Elisabeth Gruber<sup>2</sup>, Robert Ritter<sup>2</sup>, René Heller<sup>1</sup>, André Beyer<sup>3</sup>, Andrey Turchanin<sup>4</sup>, Nico Klingner<sup>1</sup>, René Hübner<sup>1</sup>, Michael Stöger-Pollach<sup>5</sup>, Henning Vieker<sup>3‡</sup>, Gregor Hlawacek<sup>1</sup>, Armin Götzhäuser<sup>3</sup>, Stefan Facsko<sup>1</sup>, Friedrich Aumayr<sup>2</sup>

<sup>1</sup> Helmholtz-Zentrum Dresden-Rossendorf, Institute of Ion Beam Physics and Materials Research, 01328 Dresden, Germany, EU

<sup>2</sup> TU Wien - Vienna University of Technology, Institute of Applied Physics, 1040 Vienna, Austria, EU

<sup>3</sup> Universität Bielefeld, Fakultät für Physik, 33615 Bielefeld, Germany, EU

<sup>4</sup> Friedrich Schiller University Jena, Institute of Physical Chemistry, 07743 Jena, Germany, EU

<sup>5</sup> TU Wien - Vienna University of Technology, USTEM, 1040 Vienna, Austria, EU

E-mail: [r.wilhelm@hzdr.de](mailto:r.wilhelm@hzdr.de)

**Abstract.** Cross-linking of a self-assembled monolayer of 1,1'-biphenyl-4-thiol by low energy electron irradiation leads to the formation of a carbon nanomembrane, which is only 1 nm thick. Here we study the perforation of these freestanding membranes by slow highly charged ion irradiation with respect to the pore formation yield. It is found that a threshold in potential energy of the highly charged ions of about 10 keV must be exceeded in order to form round pores with tunable diameters in the range of 5 - 15 nm. Above this energy threshold the efficiency for a single ion to form a pore increases from 70% to nearly 100% with increasing charge state. These findings are verified by two independent methods, namely the analysis of individual membranes stacked together during irradiation and the detailed analysis of exit charge state spectra utilizing an electrostatic analyzer.

PACS numbers: 34.35.+a, 34.50.Bw, 34.70.+e, 68.49.Sf, 68.65.-k, 79.20.Rf

*Keywords:* CNM, SAM, BPT, nanostructures, membrane, slow highly charged ion, HCI

Submitted to: *2D Mater.*

‡ Current address: CNM Technologies, Brökerstr. 8, 33602 Bielefeld

Carbon nanomembranes (CNM) made from self-assembled monolayers of different aromatic molecules are a novel type of ultrathin material which shows high stiffness with a Young's modulus of about 10 GPa [1]. CNM are also easily chemically modified [2] and may therefore serve as a functional two-dimensional material. The formation of CNM involves the cross-linking of a self-assembled monolayer of aromatic molecules by low energy electron or UV-light irradiation. The choice of aromatic molecules finally determines the thickness of the membrane in the range of 0.6 nm (naphthalene, NPHT) to 2.2 nm (hexa-*peri*-benzocoronene, HBC-CN) [3]. Even more remarkable CNM can be transformed into a single layer Graphene sheet by thermal decomposition at about 800 °C in vacuum or under protective atmosphere [4]. To integrate these membranes in devices they may be structured in a desired way by means of lithographic methods [2]. Since these membranes are typically insulating in their pristine state they are susceptible to lithography by electronic excitations, i.e. electron beams, lasers or even highly charged ions.

Typical ion beam lithography methods require large fluencies to achieve a desired material modification. When swift heavy ions [5, 6] or slow highly charged ions (HCI) [7, 8] are used instead, a single ion impact can already lead to dramatic changes in the solid which can be of interest for technological applications [9, 10, 11]. Considering the depth distribution of damage induced by these classes of ions, slow HCI are preferred for surface-only modification due to the deposition of their potential energy in a shallow region below the surface [12, 13]. The potential energy of the HCI is defined as the sum of the binding energies of all removed electrons. Several studies showed that HCI may lead to a variety of different nanostructure types, such as pit-like structures with very large corresponding sputter yields [14], nanometer sized protrusions, so called hillocks, from the surface [15, 16, 8, 17], crater structures [18, 19] or even solely changes in the local density of states [20, 21, 22, 23] depending on the target material. By reducing the solid's thickness to the range of the potential energy deposition depth (typically a few nm) also nano-pores can be created [24] and may be used as molecular sieves [25, 26]. Here we investigate the perforation of 1 nm thick, freestanding CNM by impacts of single, slow HCI. Extending our recent study [24] on the formation of nanopores in these membranes to a wider range of kinetic and potential energies and comparing with the data obtained from transmitted ions we are able to draw a phase diagram for CNM nanostructuring by slow HCI. Furthermore, we investigate the reported potential energy threshold for perforation in more detail.

Highly charged ions were produced in a room-temperature electron beam ion trap [27] which is a part of the Two-Source-Facility of the Ion Beam Center at the Helmholtz-Zentrum Dresden-Rossendorf. HCI were extracted at a constant acceleration voltage of 4.4 kV resulting in an initial kinetic ion energy of  $4.4 \text{ keV} \cdot Q$ , where  $Q$  is the ion's charge state. The ion beam was charge state separated by an analyzing magnet and focused on the target by an assembly of electrostatic lenses. An adjustable voltage difference between the beam-line (including the ion source) and the target chamber allowed the deceleration of the ions to a few keV (few  $100 \text{ V} \cdot Q$ ) final kinetic energy. A CNM was

mounted on a transmission electron microscopy (TEM) grid suspended inside the target chamber (see details below). Behind the grid an electrostatic analyzer was mounted, which allowed the determination of the charge state distribution and the corresponding energies of the transmitted ions. The base pressure inside the target chamber was in the range of  $10^{-9}$  mbar.

Irradiated samples were transferred to air and transported either to an aberration corrected FEI TITAN 80-300 TEM operated at 300 keV or to a ZEISS Orion Nanofab helium ion microscope (HIM) (both located at the Ion Beam Center) for imaging. Since microscopy analysis on these samples is very time consuming some samples were sent to the University of Bielefeld and analyzed with a ZEISS OrionPlus HIM and others to the USTEM TU Wien and imaged with a FEI TECNAI F20 TEM at 200 keV electron energy to divide rare measurement time. Some samples were analyzed at different facilities, whereas the results did not depend on the type of machine used for analysis.

The CNM used here were produced by low energy electron irradiation (cross-linking) of a self-assembled monolayer of 1,1'-biphenyl-4-thiol (BPT,  $(C_6H_5)_2SH$ ) grown on a metal substrate (for details see [28, 29]). The fully cross-linked monolayer was released from the growth substrate and transferred onto a TEM grid with an underlying holey- or lacey-carbon support film (both delivered from PLANO GMBH, Germany) for enhanced mechanical stability [30]. The CNM spans over micrometer sized holes in the carbon support film and is freestanding. The thickness of the CNM is determined by the height of the BPT monolayer and corresponds well to 1 nm [30, 1]. From the process of cross-linking we assume that a large amount (if not all) hydrogen bonds are cleaved within the BPT molecules. Additional Auger electron spectroscopy analysis excludes the presence of heavy elements above a concentration of 1 at%. Thus the CNM is treated as pure amorphous carbon material. The CNM were used as supplied without any further treatment (no annealing).

In a first step individual CNM were irradiated with Xe ions at charge states ranging from  $Q = 20$  to 40 and kinetic energies from about 2 keV to 180 keV. Applied fluencies were in the range of  $5 \cdot 10^9 \text{ cm}^{-2}$  to  $5 \cdot 10^{10} \text{ cm}^{-2}$  for all experiments resulting in 50 to 500 ion impacts per  $\mu\text{m}^2$ . For high ion charge states nanopores in the membranes were observed with a round shape and diameters in the range of a few nm, which are randomly distributed in the CNM (see Fig. 1). We attribute each observed nanopore to a single ion impact, because the probability of double impact is negligible at the fluencies applied.

A detailed study of the size dependence of the nanopores on ion's potential energy and imaging methods was published recently [24] and is now extended. Fig. 2 shows a phase diagram, i.e. combinations of kinetic and potential energies of the ions where nanopores were created (green dots). Combinations where no nanopores could be found are marked as red squares. The threshold in potential energy for nanostructuring the membranes is at about 10 - 12 keV ( $Q \approx 28$ ). A weak dependence of the threshold on kinetic energy can also be observed in Fig. 2. The fact that a charge state or potential energy threshold exists for solid surface nanostructuring is a common phenomenon

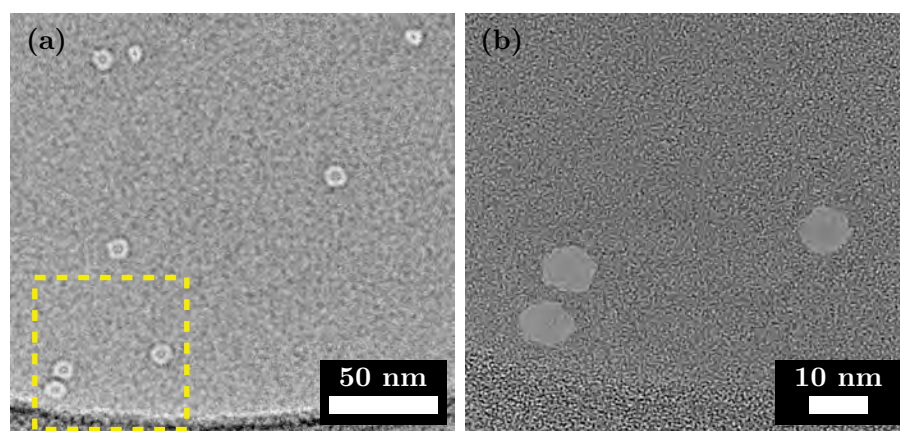


**Figure 1.** (color online) TEM images of a CNM irradiated with 176 keV  $\text{Xe}^{40+}$  ions. Left side (a) shows holes as bright spots, where the TEM was operated in underfocus to enhance contrast. The lower part of this image shows the holey-carbon support film as a darker area. The area inside the yellow square is shown with adjusted focus on the right side (b).

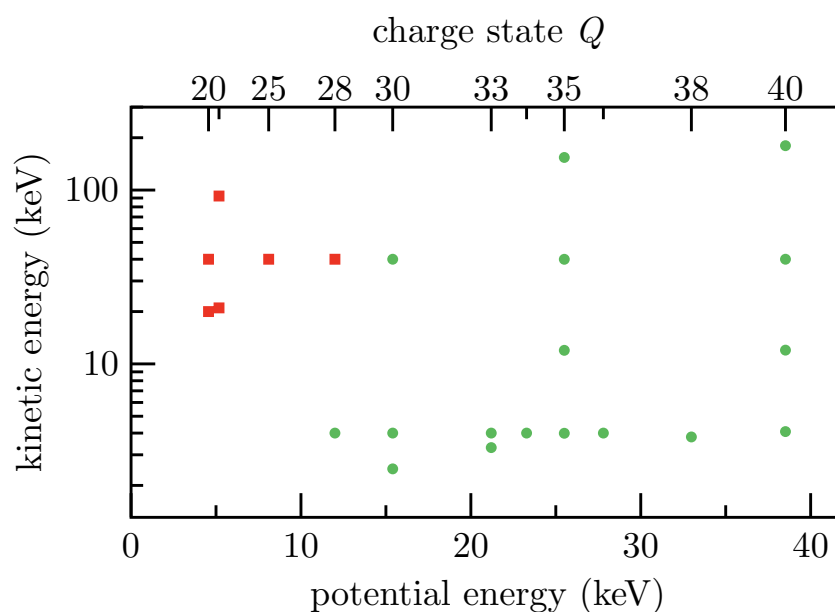


**Figure 2.** (color online) Phase diagram for pore formation by highly charged ions on carbon nanomembranes. Green dots represent combinations of kinetic and potential energy where pores were observed and red squares where **no** pores were detected. The potential energy threshold is estimated at about 10 keV.

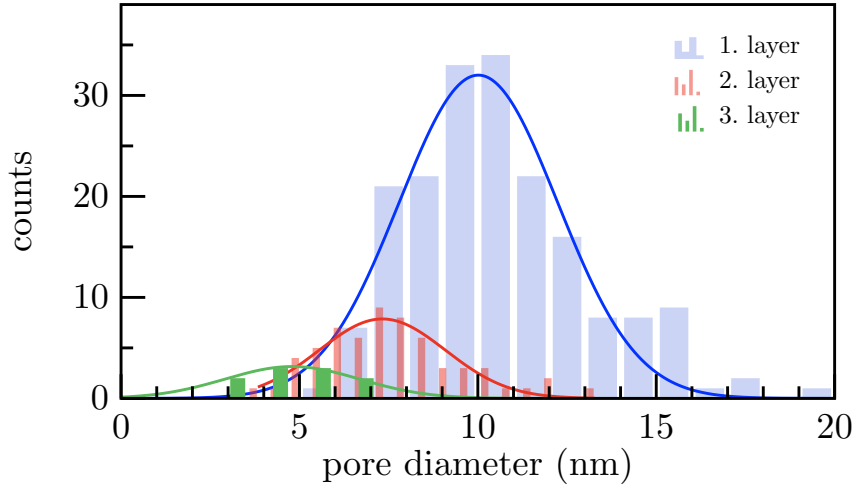


**Figure 3.** (color online) Histograms for pore sizes obtained from different CNM in a stack of three. The stack was irradiated with 40 keV  $\text{Xe}^{35+}$  ions. The mean and width of the distributions were extracted from a gaussian fit. **The bin widths are different for better representation.**

for slow HCI [7]. However, in the case of 1 nm thick CNM it could be shown, that HCI at keV kinetic energies are not completely neutralized, thus only a fraction of the potential energy is deposited in the membrane [31]. In order to determine the amount of deposited potential energy per ion two independent methods were used. Besides the analysis of the transmitted ion beam with an electrostatic analyzer, as mentioned in the experimental section and in a recent publication [31], we also used a stack of 3 CNM mounted on individual transmission electron microscopy (TEM) grids (without holey- or lacey carbon support) and squeezed together in one scanning electron microscopy holder. By irradiating this stack of CNM and imaging each layer in the stack independently, indirect access to the exit charge state distribution of each layer and the pore formation efficiency could be obtained. The key difference to direct transmission measurements is that the electrostatic analyzer covers only a small solid angle in forward direction and thus ions scattered out of the acceptance angle of the analyzer are not measured. To measure the total exit charge state distribution and determine therefore the pore formation efficiency, angle resolved measurements and subsequent integration of all the data would be needed.

Irradiated layers of a stack of three CNM were analyzed with TEM and helium ion microscopy (HIM). Surprisingly, pores could be observed not only in the first and second, but even in the third layer. Fig. 3 shows the pore size distribution for each layer of a stack of CNM irradiated with 40 keV  $\text{Xe}^{35+}$  ions. A mean pore size of 10 nm was found in the first layer (blue) and the size decreases for increasing layer number. It should be noted that each data set in Fig. 3 was obtained from a different number of images. Fig. 4 shows data from two different stacks. Both stacks were irradiated with  $\text{Xe}^{35+}$  ions at

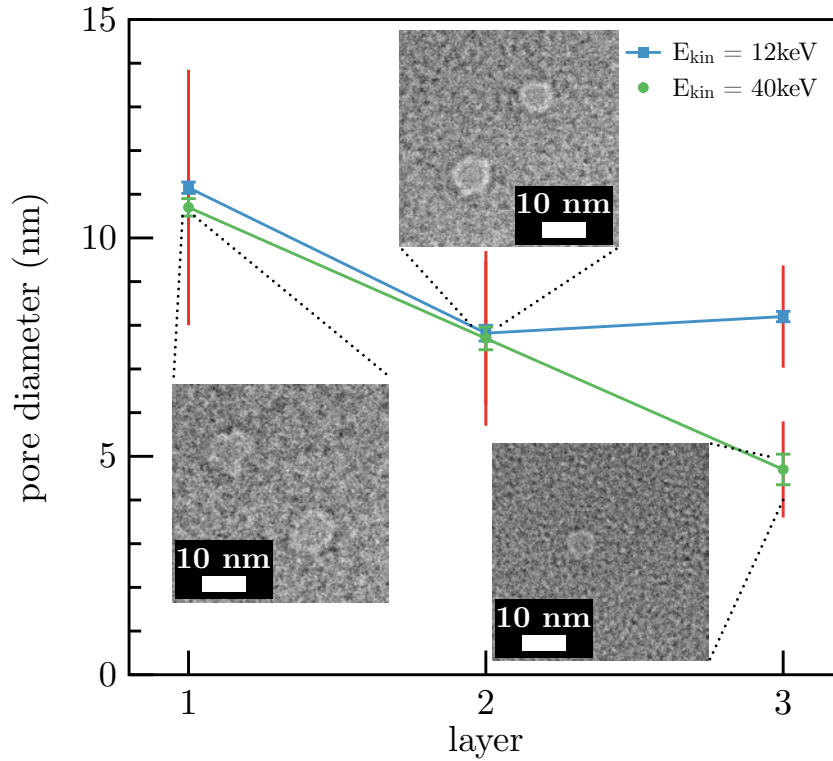


**Figure 4.** (color online) Mean pore sizes in each layer for two different stacks of three CNM. The red bars represent the width of each distribution (FWHM) and the error bars the uncertainty of the mean ( $\text{FWHM}/\sqrt{n}$ ).

different kinetic energies of 12 keV (blue squares) and 40 keV (green dots).

Fig. 5 shows an estimated pore density for the two stacks in Fig. 4. The pore density was calculated by dividing the total number of imaged pores by the total area of all images for that layer. By doing so we obtain an upper limit for the pore density, because areas where the pore density may be significantly lower were not imaged. Note that a typical TEM or HIM image has a field-of-view of  $100 \times 100 \text{ nm}^2$  to  $500 \times 500 \text{ nm}^2$  in order to observe small pores. In both cases the first layer showed a pore density which is in fair agreement with the applied ion fluence. The ion fluence was determined by measuring the ion (electrical) current on the target holder (without secondary electron suppression) and estimating the beam spot size by moving a pin hole in the target holder over the beam spot. Thus, the ion fluence is affected by significant uncertainties (relative uncertainty  $\approx 50\%$ ). Considering this fact and the limitations in statistical averaging over a large number of pores and imaged areas, our previous statement [24] about *excellent* agreement of the pore density with ion fluence is probably too strong. From Fig. 5 a decrease of pore density per layer can be observed as already indicated in Fig. 3 for both kinetic energies. Both data sets were fitted with a function  $\varrho_A(L) = \phi_0 \cdot \varepsilon^L$ , where  $\phi_0$  is - within the uncertainties discussed above - the applied ion fluence,  $L$  denotes the layer number and  $\varepsilon$  the pore formation efficiency. The best fit for the efficiency is in

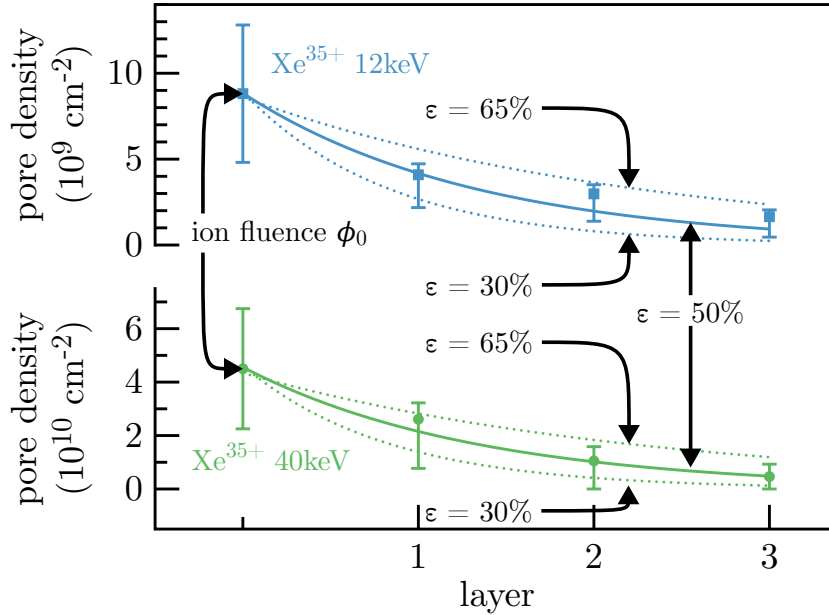


**Figure 5.** (color online) Pore density per layer for two different stacks of three CNM. The data points were fitted by an exponential function  $\phi_0 \cdot \epsilon^L$ , where  $\phi_0$  is the applied ion fluence (shown as a data point at  $L = 0$ ). An efficiency  $\epsilon$  of 50% yielded the best fit, whereas fits for efficiencies  $\epsilon = 30\%$  and  $65\%$  are indicated as dotted lines.

both cases  $\epsilon = 50\%$ . The fit indicates that (for  $E_{kin} = 10 \text{ keV} - 40 \text{ keV}$ ) at least 50% of the ions produce a pore upon impact. Fits with assumed efficiencies  $\epsilon$  of 30% and 65% are plotted as dotted curves and yield an uncertainty estimate for the efficiency. Note that an ion cannot produce a pore in more than one layer due to the high corresponding sputter yields of a few 1000 atoms. Considering typical binding energies of a few eV per atom the main fraction of the potential energy is already consumed by one pore formation. Hence, the findings indicate that the transmission through each layer leads to a bimodal exit charge state distribution. One part of the ions is transmitted in low charge states ( $Q \ll 28$ ) due to the energy deposition upon pore formation. The other part of the ions is still in sufficiently high charge states ( $Q > 28$ ) enabling pore formation in the second layer. This observation is consistent with direct transmission measurements published recently [31].

Alternatively the pore formation yield can be deduced from charge state spectra of the transmitted ion beam. Transmission spectra were obtained for ions in different incident charge states  $Q_{in}$  and the maximal available kinetic energy of  $4.4 \text{ keV} \cdot Q_{in}$  (for an example see Fig. 6). From each spectrum the relative abundance of each exit charge state was extracted and is shown in Fig. 7 as a function of the deposited potential energy (Note that the kinetic energies are different for each incident charge state.). To extract the correct abundances the data was deconvoluted from an artificial peak broadening by the electrostatic analyzer. A detailed description can be found in the Supporting

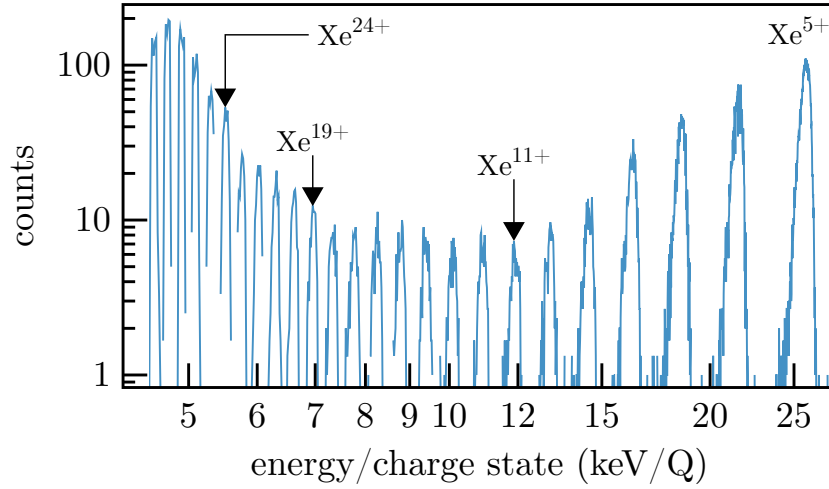


**Figure 6.** (color online) Typical transmission spectrum for highly charged Xe ions (here  $Q_{in} = 30$ ) through a CNM. Ions in the transmitted charge state  $Q = 30$  are not shown, because they result mainly from transmission through large cracks in the membrane.

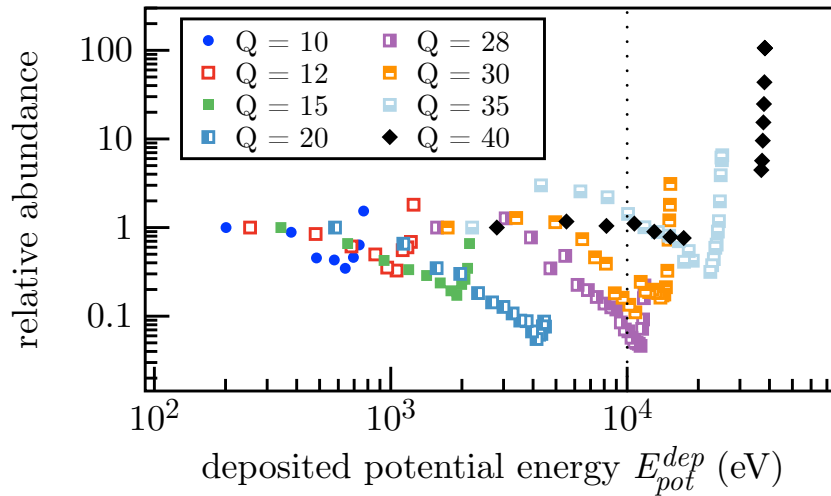


**Figure 7.** (color online) Relative abundance of deposited potential energy for Xe ions of different charge states at kinetic energies of  $4.4 \text{ keV} \cdot Q$  transmitted through a CNM. The potential energy threshold from Fig. 2 is shown as a vertical dotted line at 10 keV.

Information. The deposited potential energy is  $E_{pot}^{dep}(Q_{in}, Q_{out}) = E_{pot}(Q_{in}) - E_{pot}(Q_{out})$ , i.e. the difference of potential energy of the incident and outgoing charge states. A fraction of this deposited potential energy may be lost by emission of energetic secondary electrons and photons and may therefore not be available to the pore formation process. Bodewitz *et al.* showed recently that energetic electron emission originates also from within the material and thus potential energy deposition occurs below the surface as well [32]. The bimodal exit charge state distribution found in transmission measurements is



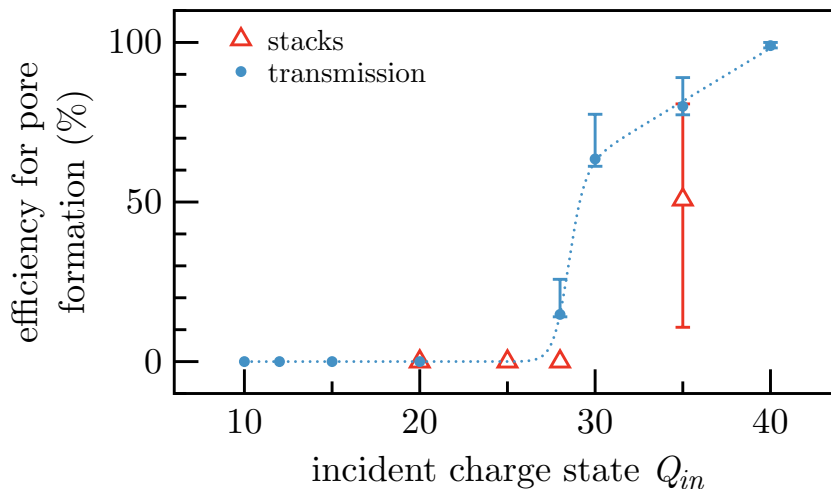


**Figure 8.** (color online) Efficiency for pore formation as a function of incident charge state and  $E_{kin}$  of  $4.4 \text{ keV} \cdot Q$  ions estimated from transmission data shown in fig 7 (blue dots) and from stack analysis (red triangles). The efficiency from transmission is a lower estimate, because the data in Fig. 7 does not contain ions with charge loss larger than 85%, i.e. single charged and neutral particles. In addition only ions transmitted in straight forward direction are accessible in the measurement.

characterized in Fig. 7 by the minimum for each data set. High relative abundance for small  $E_{pot}^{dep}$  (left of the minimum) corresponds to high exit charge states and high relative abundance for larger  $E_{pot}^{dep}$  (right of the minimum) corresponds to low exit charge states. It should be noted here, that due to experimental limitations (spectrometer voltage) the smallest observable exit charge state is  $0.15 \cdot Q_{in}$ . This means that for each set of data in Fig. 7 points with high relative abundance at the highest  $E_{pot}^{dep}$  are missing, because neutral and almost neutral particles could not be measured.

However, by combining the empirical finding of Fig. 2 that the potential energy should be larger than about 10 keV in order to form pores in CNM and the relative abundance of potential energy deposition with values larger than 10 keV from Fig. 7 (threshold marked by the dotted line) we can directly estimate a pore formation efficiency. Fig. 8 shows the efficiency per ion to form a pore as function of the incident charge state and kinetic energies of  $4.4 \text{ keV} \cdot Q_{in}$ . The values of efficiency are given by the quotient of the summed abundance of  $E_{pot}^{dep} > 10 \text{ keV}$  and the summed abundance of all transmitted ions. The efficiency is 0 up to around  $Q_{in} = 28$  and increases than rapidly to about 70% at  $Q = 30$ . The rapid increase is again evidence that the threshold for nanostructuring of surfaces and membranes is sharp in terms of potential energy. For even larger charge states the efficiency increases linearly with charge state and reaches about 100% for  $Q = 40$ . Additionally the deduced efficiencies estimated from the stack experiments are shown as red triangles. Data for  $Q < 30$  is taken from single layer irradiations where no pores were observed at 40 keV kinetic energy (see Fig. 2).

To estimate the importance of the potential energy in the sputter process the observed sputter yield may be compared to values obtained from a standard binary collision approximation simulation (TRIM). The sputter yield deduced from this simulation results exclusively from elastic collisions and is about 3 orders of magnitude below the observed yield. Even for a charge state enhanced nuclear scattering cross-section [33] the sputter yield from elastic collisions may not increase significantly due to the small thickness of the membrane and preferred forward scattering of heavy xenon projectiles on light carbon atoms. Thus, the potential energy is the driving force for the sputtering from the CNM together with possible enhanced *electronic* losses. Kinetically assisted potential sputtering was recently observed on a polymer - namely PMMA [34] - and alkali halides such as KBr [14], where also some contribution of kinetic losses to electronic excitations may be assumed. Finally, the role of the kinetic energy deposition in the pore formation process is not entirely clear, limiting the interaction time on the one hand but delivers energy to the nuclear and possibly to the electronic system on the other hand.

In this paper we showed that single slow HCI can be used to perforate CNM with an efficiency of close to 100% when the ion's charge state is considerably higher than a threshold value of about  $Q_{th} = 28$ . This information can be derived from direct transmission measurements and independently from imaging a stack of several irradiated layers of CNM. It is shown that directly from charge exchange measurements information about structural changes in a material can be gained.

## Acknowledgments

Financial support from the Deutsche Forschungsgemeinschaft (DFG) (project-no. HE 6174/1-1) and from the Austrian FWF (project-no. I 1114-N20) is acknowledged.

## References

- [1] Turchanin A and Götzhäuser A 2012 *Prog Surf Sci* **87** 108–162
- [2] Beyer A, Godt A, Amin I, Nottbohm C T, Schmidt C, Zhao J and Götzhäuser A 2008 *Phys. Chem. Chem. Phys.* **10** 7233–7238
- [3] Angelova P, Vieker H, Weber N E, Matei D, Reimer O, Meier I, Kurasch S, Biskupek J, Lorbach D, Wunderlich K, Chen L, Terfort A, Klapper M, Müllen K, Kaiser U, Götzhäuser A and Turchanin A 2013 *ACS Nano* **7** 6489–97
- [4] Matei D G, Weber N E, Kurasch S, Wundrack S, Woszczyna M, Grothe M, Weimann T, Ahlers F, Stosch R, Kaiser U and Turchanin A 2013 *Adv. Mater.* **25** 4146–4151
- [5] Khalfaoui N, Rotaru C C, Bouffard S, Toulemond M, Stoquert J P, Haas F, Trautmann C, Jensen J and Dunlop A 2005 *Nucl Instrum Methods Phys Res Sect B* **240** 819–828
- [6] Ochedowski O, Osmani O, Schade M, Bussmann B K, Ban-d'Etat B, Lebius H and Schleberger M 2014 *Nat Commun* **5** 3913
- [7] Aumayr F, Facsko S, El-Said A S, Trautmann C and Schleberger M 2011 *J Phys Condens Matter* **23** 393001
- [8] El-Said A S, Wilhelm R A, Heller R, Facsko S, Lemell C, Wachter G, Burgdörfer J, Ritter R and Aumayr F 2012 *Phys Rev Lett* **109** 117602

- [9] Olivares J, García G, García-Navarro A, Agulló-López F, Caballero O and García-Cabañes A 2005 *Appl Phys Lett* **86** 183501
- [10] Sanz R, Jensen J, Johansson A, Skupinski M, Possnert G, Boman M, Hernandez-Vélez M, Vazquez M and Hjort K 2007 *Nanotechnology* **18** 305303
- [11] Krashennikov A V and Nordlund K 2010 *J Appl Phys* **107** 071301
- [12] Arnau A, Aumayr F, Echenique P M, Grether M, Heiland W, Limburg J, Morgenstern R, Roncin P, Schippers S, Schuch R, Stolterfoht N, Varga P, Zouros T J M and Winter H P 1997 *Surf Sci Rep* **27** 113–239
- [13] Schenkel T, Hamza A V, Barnes A V and Schneider D H 1999 *Prog Surf Sci* **61** 23–84
- [14] Heller R, Facsko S, Wilhelm R A and Möller W 2008 *Phys Rev Lett* **101** 096102
- [15] Minniti R, Ratliff L P and Gillaspay J D 2001 *Physica Scripta* **T92** 22–26
- [16] El-Said A S, Heller R, Meissl W, Ritter R, Facsko S, Lemell C, Solleder B, Gebeshuber I C, Betz G, Toulemonde M, Möller W, Burgdörfer J and Aumayr F 2008 *Phys Rev Lett* **100** 237601
- [17] Zhou P, Zhang H Q, Zhang Q, Liu Z, Guan S, Wang G, Zhou C, Jia J, Lv X, Shao J, Cui Y, Chen L and Chen X 2013 *Nucl Instrum Methods Phys Res Sect B* **307** 221–224
- [18] Tona M, Watanabe H, Takahashi S, Nakamura N, Yoshiyasu N, Sakurai M, Terui T, Mashiko S, Yamada C and Ohtani S 2007 *Surf Sci* **601** 723–727
- [19] Tona M, Fujita Y, Yamada C and Ohtani S 2008 *Phys Rev B* **77** 155427
- [20] Terada M, Nakamura N, Nakai Y, Kanai Y, Ohtani S, Komaki K and Yamazaki Y 2005 *Nucl Instrum Methods Phys Res Sect B* **235** 452–455
- [21] Tona M, Watanabe H, Takahashi S, Fujita Y, Abe T, Jian S, Nakamura N, Yoshiyasu N, Yamada C, Sakurai M and Ohtani S 2007 *J Phys: Conf Ser* **58** 331–334
- [22] Ritter R, Kowarik G, Meissl W, Suss L, Maunoury L, Lebius H, Dufour C, Toulemonde M and Aumayr F 2010 *Nucl Instrum Methods Phys Res Sect B* **268** 2897–2900
- [23] Ritter R, Shen Q, Wilhelm R A, Heller R, Ginzl R, López-Urrutia J R C, Facsko S, Teichert C and Aumayr F 2013 *Nucl Instrum Methods Phys Res Sect B* **315** 252–256
- [24] Ritter R, Wilhelm R A, Stöger-Pollach M, Heller R, Mücklich A, Werner U, Vieker H, Beyer A, Facsko S, Gözlhäuser A and Aumayr F 2013 *Appl Phys Lett* **102** 063112
- [25] Noack M, Kölsch P, Schäfer R, Toussaint P and Caro J 2002 *Chem. Eng. Technol.* **25** 221–230
- [26] Tong H D, Jansen H V, Gadgil V J, Bostan C G, Berenschot E, Van Rijn C J M and Elwenspoek M 2004 *Nano Lett.* **4** 283–287
- [27] Zschornack G, Kreller M, Ovsyannikov V P, Grossman F, Kentsch U, Schmidt M, Ullmann F and Heller R 2008 *Rev Sci Instrum* **79** 02A703
- [28] Turchanin A, Käfer D, El-Desawy M, Wöll C, Witte G and Gözlhäuser A 2009 *Langmuir* **25** 7342–7352
- [29] Angelova P, Vieker H, Weber N E, Matei D, Reimer O, Meier I, Kurasch S, Biskupek J, Lorbach D, Wunderlich K, Chen L, Terfort A, Klapper M, Mullen K, Kaiser U, Gözlhäuser A and Turchanin A 2013 *Acs Nano* **7** 6489–6497
- [30] Turchanin A, Beyer A, Nottbohm C T, Zhang X H, Stosch R, Sologubenko A, Mayer J, Hinze P, Weimann T and Gözlhäuser A 2009 *Adv Mater* **21** 1233–1237
- [31] Wilhelm R A, Gruber E, Ritter R, Heller R, Facsko S and Aumayr F 2014 *Phys Rev Lett* **112** 153201
- [32] Bodewits E, Hoekstra R, Dobes K and Aumayr F 2014 *Phys. Rev. A* **90** 052703
- [33] Biersack J 1993 *Nucl Instrum Methods Phys Res Sect B* **8081** 12–15
- [34] Ritter R, Wilhelm R A, Ginzl R, Kowarik G, Heller R, El-Said A S, Papaléo R M, Rupp W, López-Urrutia J R C, Ullrich J, Facsko S and Aumayr F 2012 *Europhys Lett* **97** 13001